

Tropical cyclones near landfall can induce their own intensification through feedbacks on radiative forcing

Charlie C. F. Lok ¹, Johnny C. L. Chan ¹✉ & Ralf Toumi ²

Rapid intensification of near-landfall tropical cyclones is very difficult to predict, and yet has far-reaching consequences due to their disastrous impact to the coastal areas. The focus for improving predictions of rapid intensification has so far been on environmental conditions. Here we use the Coupled-Ocean-Atmosphere-Wave-Sediment Transport Modeling System to simulate tropical cyclones making landfall in South China: Nida (2016), Hato (2107) and Mangkhut (2018). Two smaller storms (Hato and Nida) undergo intensification, which is induced by the storms themselves through their extensive subsidence ahead of the storms, leading to clear skies and strong solar heating of the near-shore sea water over a shallow continental shelf. This heating provides latent heat to the storms, and subsequently intensification occurs. In contrast, such heating does not occur in the larger storm (Mangkhut) due to its widespread cloud cover. This results imply that to improve the prediction of tropical cyclone intensity changes prior to landfall, it is necessary to correctly simulate the short-term evolution of near-shore ocean conditions.

¹School of Energy and Environment, City University of Hong Kong, Hong Kong, China. ²Space and Atmospheric Physics Group, Imperial College London, London, UK. ✉email: Johnny.Chan@cityu.edu.hk

Because the damages caused by a tropical cyclone (TC) at landfall are very much related to its maximum winds, referred to as intensity, the prediction of TC intensity is of utmost importance. Previous studies^{1–4} to understand and improve the prediction of intensification focused on examining the environmental forcings. However, the skill in intensity prediction has not improved much in the last few decades despite substantial increases in data availability and enhancements in weather prediction technologies such as data assimilation^{5,6}.

Typhoon Hato made landfall near Macau along the South China coast on 23 August 2017, causing tremendous damage and at least 25 fatalities⁷. Just prior to its landfall, it underwent rapid intensification from 60 to 100 knots within 24 h. Most operational numerical weather prediction models failed to predict this intensification process. Pun et al.⁸ suggested that the rapid intensification is likely related to the very warm sea water over the shallow continental shelf that provides the necessary enthalpy to the TC to intensify rapidly. In general, Ekman pumping will cause upwelling of sub-surface water, which is cooler, and hence weakens a TC^{9–13}. However, because of the shallowness of the ocean due to the presence of the continental shelf (with a depth of <200 m), such upward mixing does not lead to any cooling and the TC can therefore intensify^{8,14}. The question is why the sea water can be so warm in the first place.

We hypothesize that the extensive subsidence ahead of the TC reduces the cloud cover there¹⁵, thus allowing strong shortwave radiation to warm the ocean surface. This stable area of subsidence is also characterized by low winds and thus low surface heat loss. Because near the South China coast, the continental shelf is relatively shallow, the water can be heated up within a short period of time. The increase in water temperature then provides a substantial increase in enthalpy to the TC as it

moves over this warm water, and hence intensification occurs. To test this hypothesis, the Coupled-Ocean-Atmosphere-Wave-Sediment Transport Modeling System version 3.2 revision 1192 (hereafter COAWST)¹⁶ is run under three conditions: the control experiment with all the physics; the NORAD experiment with ocean radiative heating and cooling disabled; and the NORAD-t18 experiment with the radiation term in the ocean model turned off for the first local day. The results show that a TC making landfall at a coastal area with a shallow continental shelf can self-induce intensification under certain conditions, and are presented in the following section.

Results and discussions

Self-induced near landfall intensification. Except at the beginning of the simulations, all three experiments simulate the track of Hato very well, especially near its landfall (Fig. 1a). The intensification process is also reproduced in these experiments, with the TC deepening from 1000 to 973 hPa just before it enters the continental shelf (Fig. 1d). The control TC further intensifies to 970 hPa (blue dashed line in Fig. 1d) with maximum sustained wind reaching 95 knots near the time of landfall. On the other hand, in the NORAD experiment, the TC intensifies less by ~5 hPa during the same period (green dotted line in Fig. 1d) with maximum wind of only 80 knots instead, while the TC in NORAD-t18 has a similar intensity as that in NORAD (purple dash-dotted line in Fig. 1d).

To understand how solar radiation might contribute to the difference in the intensities in the three experiments, we first analyze the results in the control experiment. Along the edge of the continental shelf between Hainan and Taiwan Islands, the sea surface temperature (SST) generally cools down by 2–3 °C during the passage of Hato (between 22 August 12 UTC and 23 August

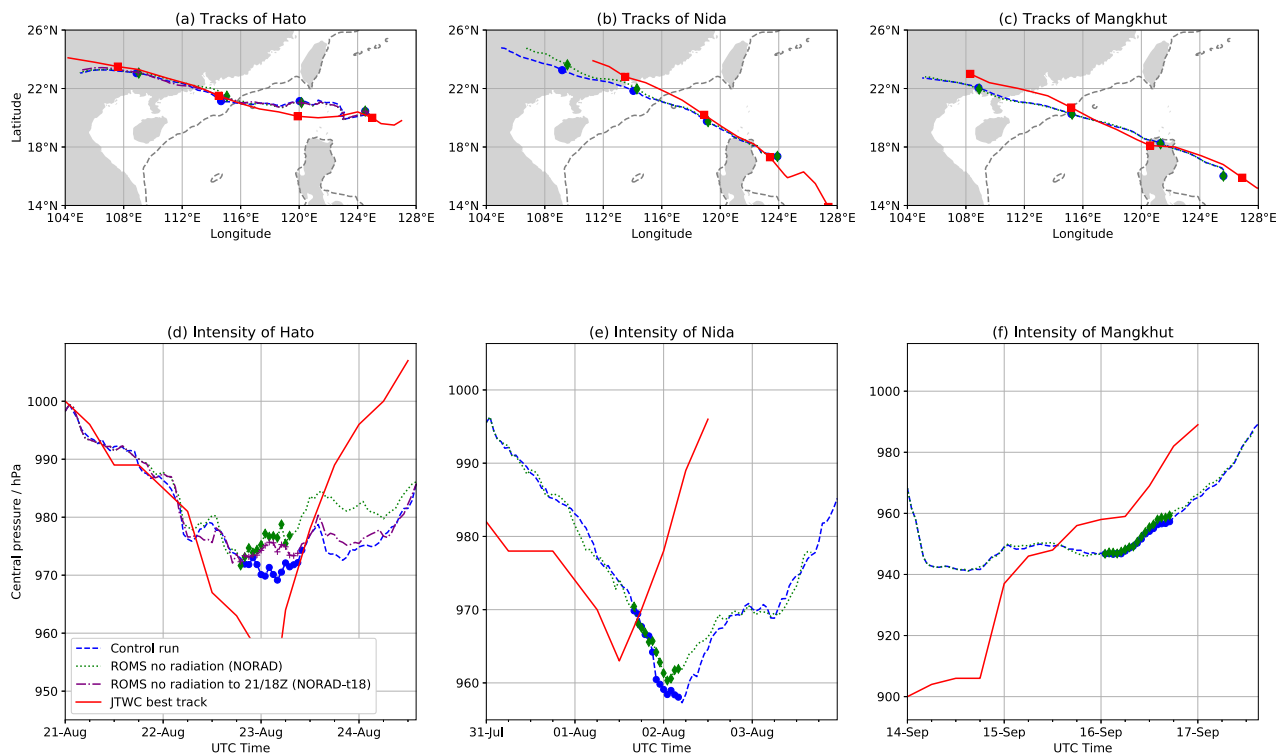


Fig. 1 Simulated tracks and intensities of TCs. Tracks of Typhoons **a** Hato, **b** Nida, and **c** Mangkhut from the JTWC best track (red solid), the control (blue dashed), the NORAD (green dotted) and NORAD-t18 (purple dash-dotted) experiments. Their positions at 00 UTC are marked by squares (JTWC), circles (control), diamonds (NORAD) and crosses (NORAD-t18) respectively. Ocean isobaths of 200 m are drawn in gray dashes. Time series of minimum sea-level pressure in hPa of **d** Hato, **e** Nida and **f** Mangkhut, with markers indicating their passages over the continental shelf.

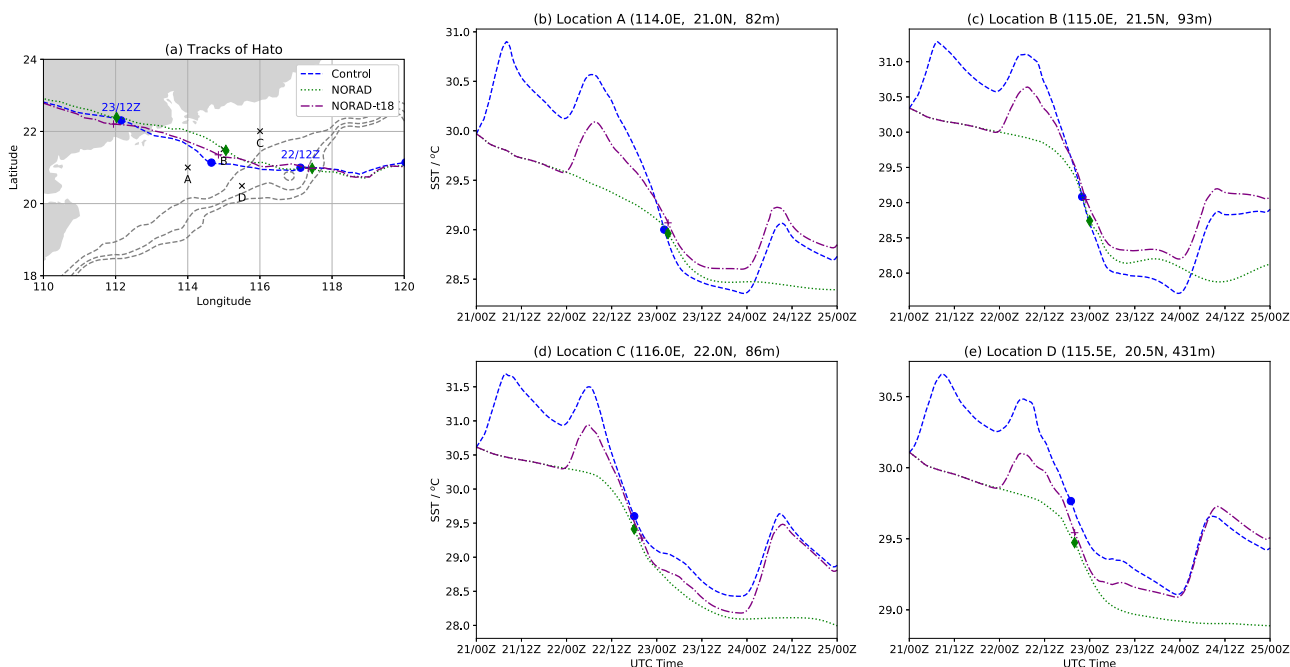


Fig. 2 Time series of SST during the passage of Typhoon Hato. **a** Simulated tracks of Typhoon Hato with makers at every 12 h, black crosses at the locations of the time series, and ocean isobaths of 200, 600, and 1000 m in gray dashes. **b–e** Time series of SST at the four locations crossed in **a** along the edge of continental shelf during the passage of Typhoon Hato in the control (blue dashed), NORAD (green dotted) and NORAD-t18 (purple dash-dotted) experiments. Markers indicate Typhoon Hato’s closest time of approach.

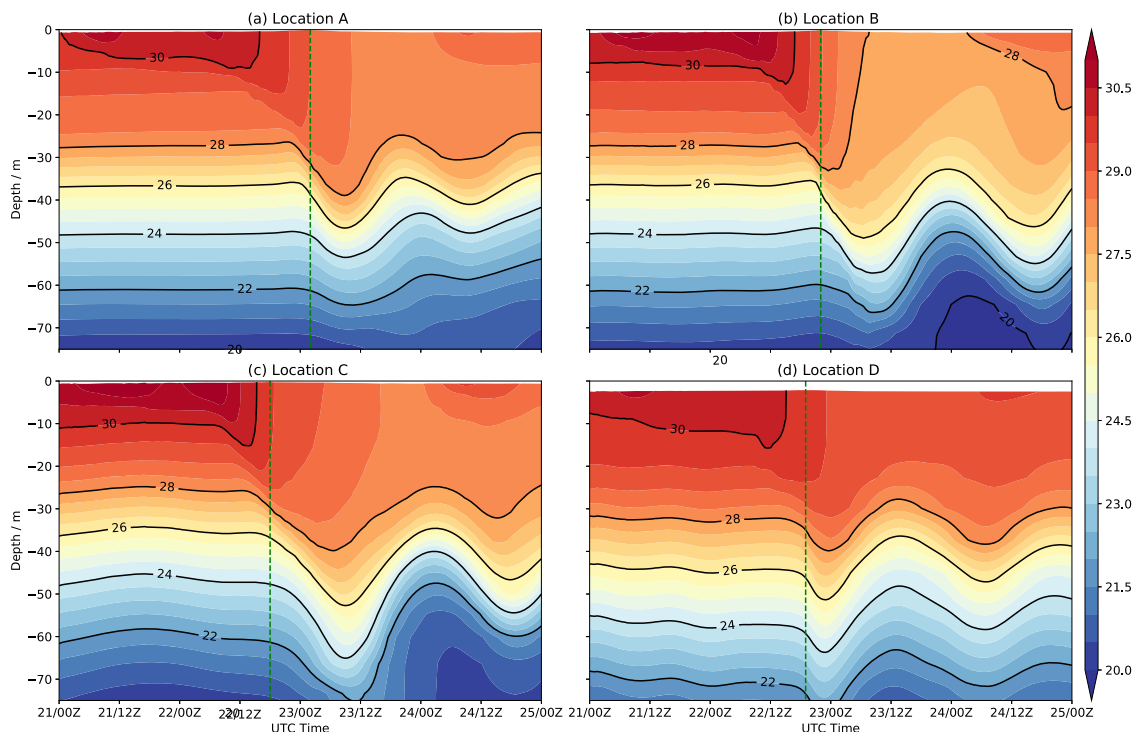


Fig. 3 Cross sections of ocean temperature during the passage of Typhoon Hato. Hovmöller diagrams of vertical ocean temperature profile in °C of the control experiment of Typhoon Hato at the four locations along the edge of continental shelf specified in Fig. 2a for **a** left hand side of the track, **b** over the track, **c** right hand side of the track, and **d** deeper ocean. Green dashes represent the closest time of approach to Typhoon Hato.

12 UTC in locations A, B, and C of Fig. 2), a phenomenon in agreement with previous studies^{9,14,17}. On the other hand, a strong diurnal signal (~0.8 °C) is observed in the same locations ahead of Hato (21 and 22 August). More importantly, the

underlying ocean mixed layer is subsequently warmed by 1 °C during the same period (Fig. 3).

To diagnose the causes(s) of such warming in the ocean mixed layer (defined as within 0.8 °C of SST)¹⁸, the various terms in the

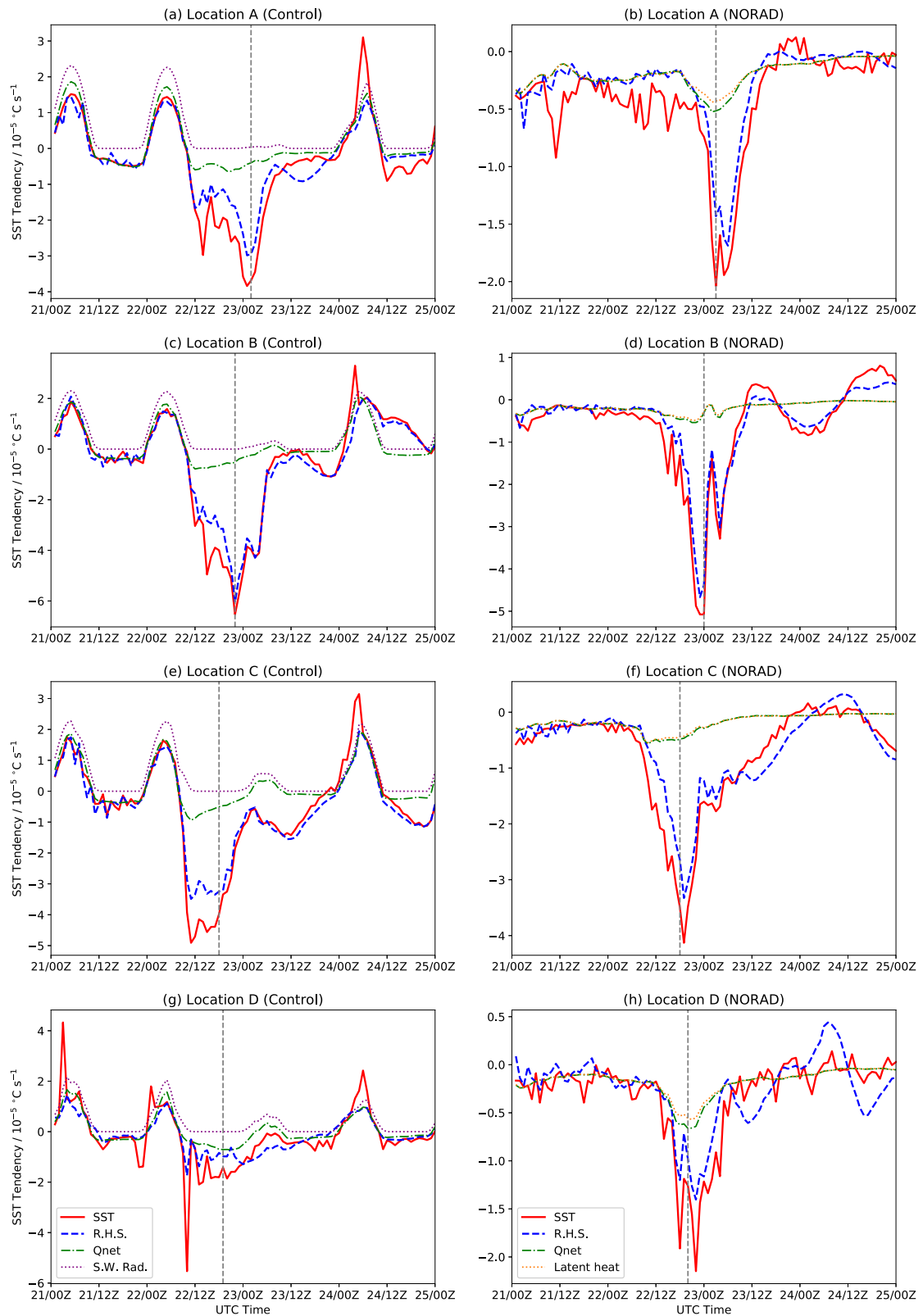


Fig. 4 Time series of various terms in the SST tendency equation. Time series of ocean mixed layer temperature change rate (red solid), the sum of right-hand side of Eq. 1 (blue dashed), net air-sea heat flux Q_{net} (green dotted), shortwave radiative heating (purple dash-dotted) and latent heat flux (orange dash-dotted) from the **a, c, e, g** control and **b, d, f, g** NORAD experiments of Typhoon Hato at locations **a, b A, c, d B, e, f C** and **g, h D** specified in Fig. 2a. Units are in 10^{-5} °C per second, and positive (negative) indicates heat gain (loss) by the ocean. Gray dashes indicate Typhoon Hato's closest time of approach.

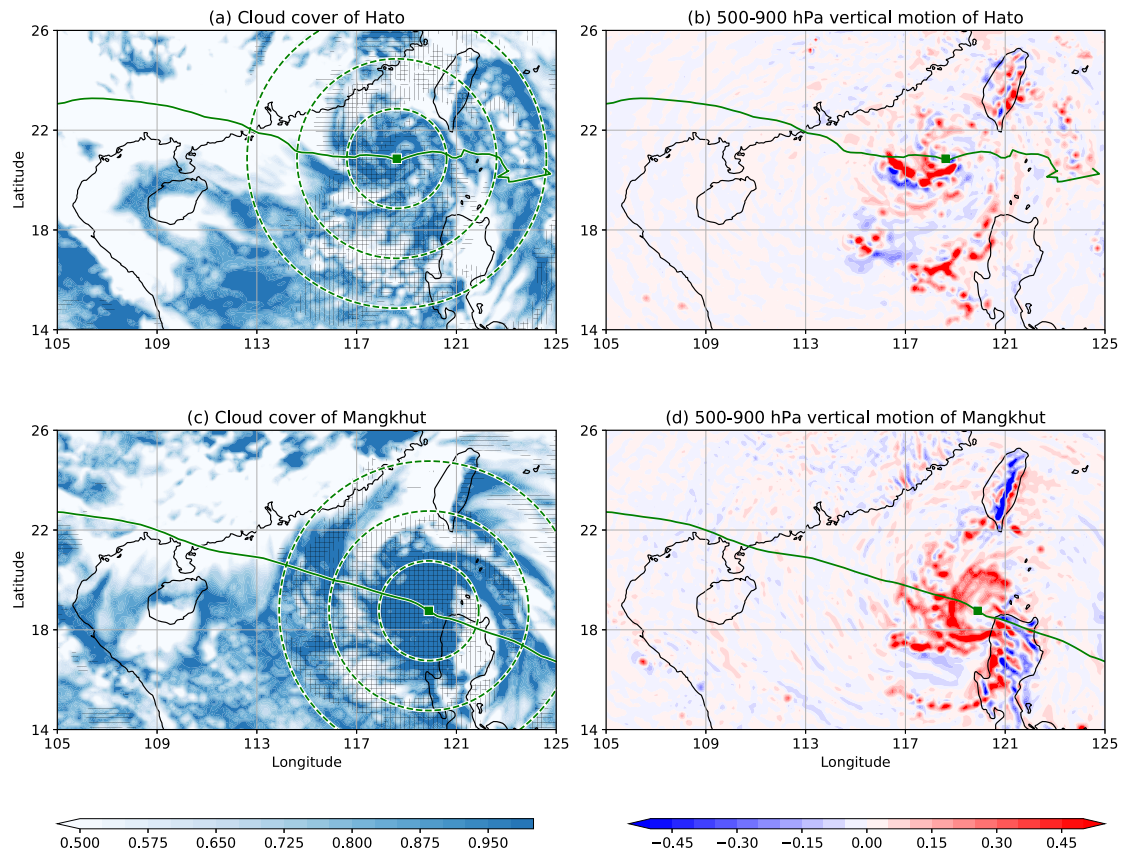


Fig. 5 Simulated cloud cover and vertical motion for Typhoons Hato and Mangkhut. Simulated **a, c** low-level cloud fractions and **b, d** 500–900 hPa layer mean vertical motion in m s^{-1} at 06 UTC on **a, b** 22 August 2017 for Typhoon Hato and **b, c** 15 September 2018 for Mangkhut. Mid- and high-level cloud fractions exceeding 80% are hatched with blue horizontal and red vertical lines respectively. Green lines are the corresponding tracks, with squares indicating the position of the TCs. 200, 400, and 600 km distances from the TCs are drawn in green dashed lines.

temperature tendency equation¹⁹ are examined as follows:

$$\frac{\partial T_m}{\partial t} = -\vec{V} \cdot \nabla T_m - (w + w_e) \frac{T_m - T_b}{h} + \kappa \nabla^2 T_m + \frac{Q_{\text{net}}}{\rho c_p h} \quad (1)$$

where T_m is ocean mixed layer temperature, T_b is the temperature just below the mixed layer, \vec{V} is the horizontal ocean current vector, w the vertical velocity, w_e the entrainment velocity, h the depth of ocean mixed layer, κ is horizontal viscosity coefficient, Q_{net} the net heat flux at the air–sea boundary, which is the sum of shortwave and longwave radiative fluxes, and latent and sensible heat fluxes at the sea surface assuming no solar radiation penetrating further below, ρ the sea-water density (1025 kg m^{-3}), and c_p specific heat of sea-water ($3850 \text{ J kg}^{-1} \text{ }^\circ\text{C}^{-1}$).

Time series of the sum of right-hand side of Eq. 1 (blue lines in Fig. 4) and the simulated mixed layer temperature change rates (red lines in Fig. 4) from the control experiment are in good agreement among the four locations, affirming that the tendency equation can be used to diagnosis the cause(s) of the SST warming. It is further demonstrated that the shortwave radiation term (purple dotted lines in Fig. 4a, c, e, g) dominates the sum of right-hand side of Eq. 1 on 21 and 22 August, which suggests that solar radiation is the primary heat source^{20,21}. The effect of solar heating in location A, B and C is larger than location D due to the shallower water. As such, there is substantial SST warming near the coast.

The reason for the dominant contribution of shortwave radiation to the net heating is because the atmosphere over the continental shelf to the northwest of the TC is generally cloud-

free (see Fig. 5a) and stable with weak surface winds due to extensive subsidence in the region¹⁵ (Fig. 5b). As such, solar radiation is able to reach the sea surface, and warms up the underneath ocean, which is relatively shallow. This warm pool of water over the continental shelf then provides enthalpy for Hato to intensify rapidly just before making landfall.

In contrast, in the NORAD run, the near-shore SST warming no longer appears and the latent heat flux becomes the dominant term of right-hand side of Eq. 1 instead (orange dotted lines in Fig. 4b, d, f, h). The SST in the NORAD run is $\sim 0.5\text{--}1 \text{ }^\circ\text{C}$ colder than that in the control (Fig. 2), and the latent heat flux provided to the atmosphere before the passage of Hato is smaller (Fig. 6). As there is less energy available to Hato, the TC does not intensify as much as in the control run. Even if the ocean radiative heating is only switched off for one local day (the NORAD-t18 run), SST over the continental shelf is still $\sim 0.5 \text{ }^\circ\text{C}$ colder by the time Hato entered the continental shelf (Fig. 2). As Hato moves closer to the land, one day is not enough to warm up the ocean to the same temperature as the control does in 2 days. Both the NORAD and NORAD-t18 runs confirm that solar radiation contributes substantially to increasing the SST over the continental shelf to the northwest of Hato, which subsequently leads to the intensification of Hato.

To be more confident that the self-induced intensification of Hato is not an isolated case, we examine another typhoon, Nida (2016) that made landfall in a similar location (Fig. 1b). The NORAD experiment gives a minimum sea-level pressure $\sim 5 \text{ hPa}$ higher than that in the control (Fig. 1e). The SST time series in the control experiment (Fig. 7) is similar to the case of Hato (cf.

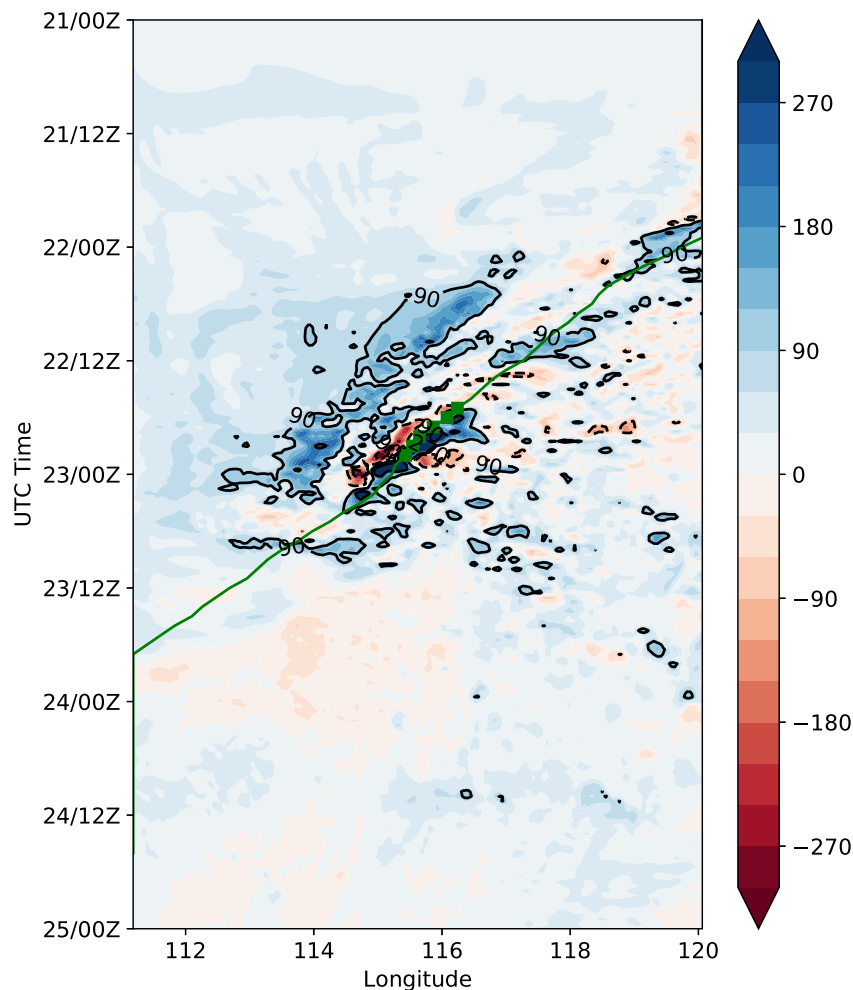


Fig. 6 Differences in latent heat flux between the control and NORAD runs. Hovmöller diagram of latent heat flux differences in W m^{-2} between the control and NORAD experiments of Typhoon Hato along the edge of the continental shelf between Hainan and Taiwan islands. Green lines represent the nearest point of the line to Hato, with squares indicating the distance less than 10 km.

Fig. 2), with substantial heating ahead of Nida, and hence its intensification (Fig. 1e). The difference between the two experiments also shows not much heating in the NORAD experiment. These results substantiate the validity of the hypothesis of self-induced intensification.

Limitation from cloud cover on self-induced intensification.

The results from these experiments substantiate the hypothesis that it is indeed possible for a TC to self-induce intensification. The crucial factor seems to be whether the atmosphere ahead of the TC over the continental shelf is cloud free. In 2018, another typhoon, Mangkhut, moved over almost the same area along the South China coast (Fig. 1c), which therefore provided an opportunity to test this assertion.

The same control and NORAD experiments as in the case of Hato are run. Although the simulated tracks are slightly west of the actual one (Fig. 1c), the vortices move over the continental shelf in a way similar to the case of Hato. However, no difference can be found between these experiments in their simulated intensities (Fig. 1f). The almost identical intensities in the two experiments are also reflected in the SST time series (Fig. 8), with the difference being $<0.5^\circ\text{C}$ most of the time.

The reason for this lies in the fact that the simulated cloud cover ahead of Mangkhut is very extensive (Fig. 5c). As a result, solar radiation cannot reach the ocean over the continental shelf to heat the water up. Turning on the radiation term would not contribute much to the total heating, and hence the SST distributions in the two experiments are similar.

Conclusion

To summarize, this study demonstrates that a TC near the coast could self-induce its own intensification if the following conditions are met: (1) there exists a relatively shallow continental shelf so that water can be heated by solar radiation within the daylight hours, and (2) the extent of the cloud cover ahead of the TC is small so that the ocean water over the continental shelf can be exposed to solar radiation. Of course, atmospheric factors such as vertical wind shear²² should also support its intensification.

This result also suggests that in predicting whether a TC will likely intensify before it makes landfall along a coast with a shallow continental shelf, it is important to predict the cloud cover and the ocean response to this ahead of the TC. For numerical model predictions, it is clear that a fully-coupled ocean model is necessary so that the SST response to cloud cover can be

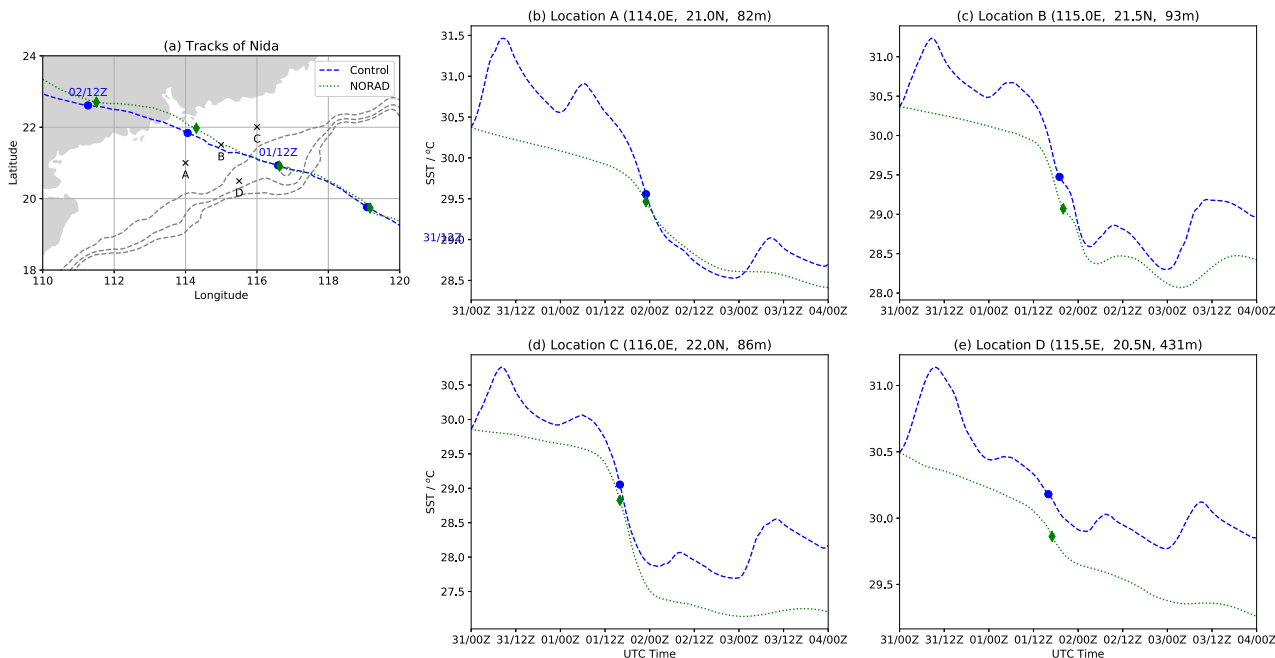


Fig. 7 Time series of SST during the passage of Typhoon Nida. **a** Simulated tracks of Typhoon Nida with markers at every 12 h, black crosses at the locations of the time series, and ocean isobaths of 200, 600, and 1000 m in gray dashes. **b–e** Time series of SST at the four locations crossed in **a** along the edge of continental shelf during the passage of Typhoon Nida in the control (blue dashed) and NORAD (green dotted) experiments. Markers indicate Typhoon Nida’s closest time of approach.

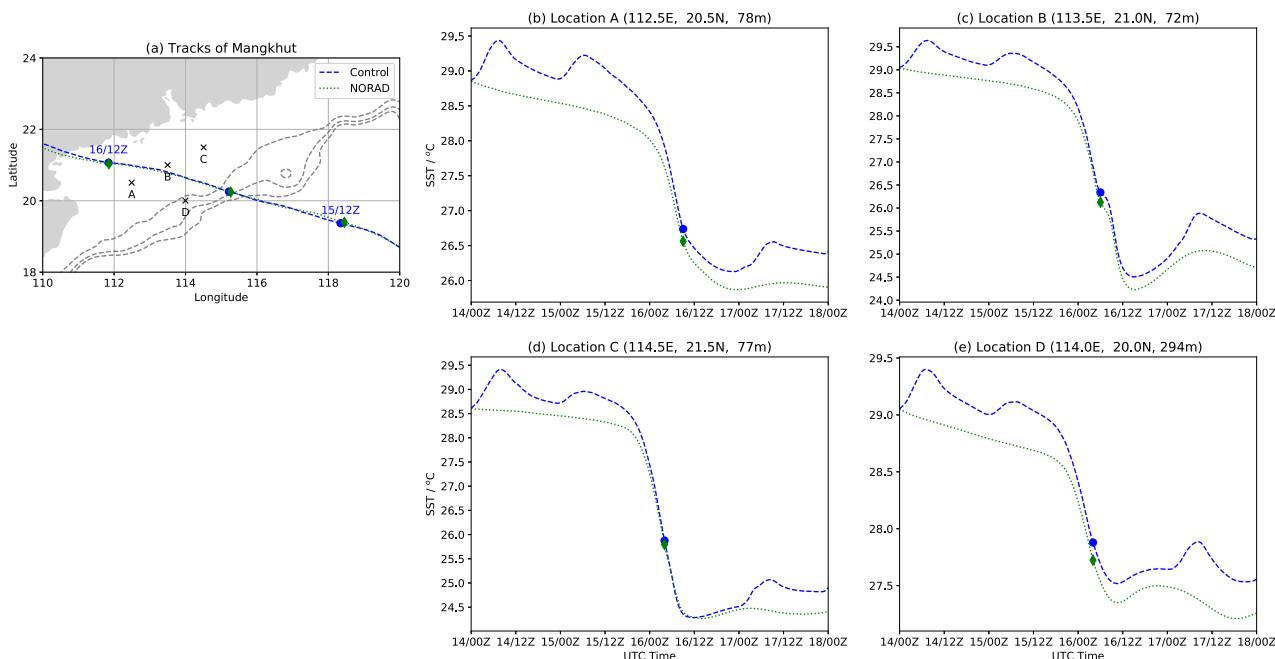


Fig. 8 Time series of SST during the passage of Typhoon Mangkhut. **a** Simulated tracks of Typhoon Mangkhut with markers at every 12 h, black crosses at the locations of the time series, and ocean isobaths of 200, 600, and 1000 m in gray dashes. **b–e** Time series of SST at the four locations crossed in **a** along the edge of continental shelf during the passage of Typhoon Mangkhut in the control (blue dashed) and NORAD (green dotted) experiments. Markers indicate Typhoon Mangkhut’s closest time of approach.

predicted. The ability of models to predict cloud cover ahead of the TC will also need to be examined.

Methods

The COAWST modeling system. The air-sea-wave coupled model used in this study is COAWST version 3.2 revision 1192¹⁶. It consists of three models: the Weather Research and Forecasting Model version 3.7.1 (hereafter WRF)²³, the

Regional Ocean Modeling System revision 838 (hereafter ROMS)²⁴ and the Simulating Waves Nearshore model version 41.01AB (hereafter SWAN)²⁵. The three models are connected by the Model Coupling Toolkit version 2.6.0 (hereafter MCT)²⁶ to exchange information.

The WRF model solves the compressible, non-hydrostatic Euler equations of the atmosphere, with the following physical packages applied for subgrid processes: the WRF Single Movement class 6 scheme²⁷ for microphysics, the Yonsei University scheme²⁸ for the planetary boundary layer, Tiedtke scheme²⁹ for

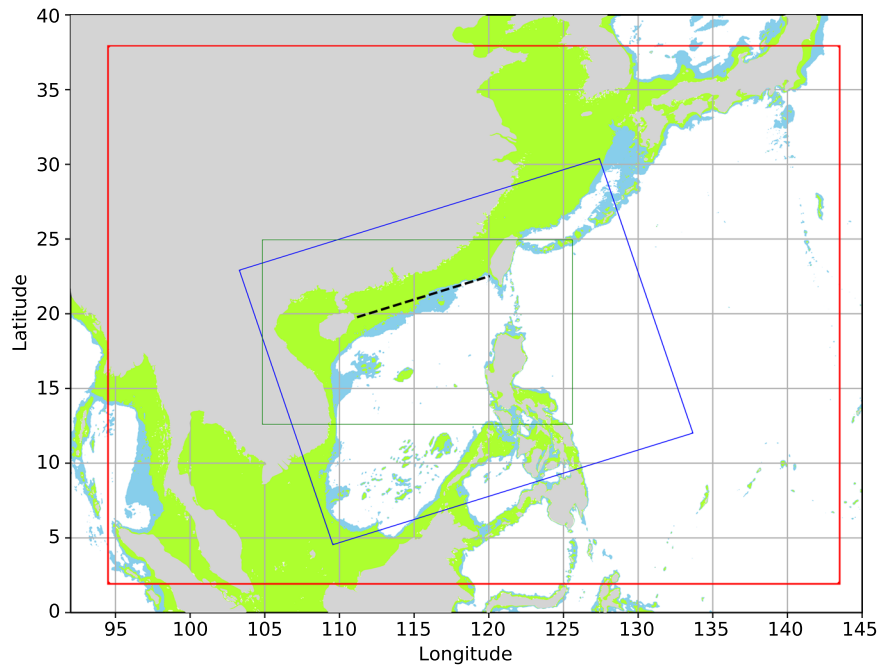


Fig. 9 COAWST domains. Domains of the outer (red box) and inner (green box) grids of WRF, and ROMS and SWAN (blue box). Green and blue colors denote ocean depths of <200 m and between 200 and 1000 m, respectively. Black dashed line represents the data line used in the Hovmöller diagrams in Fig. 6.

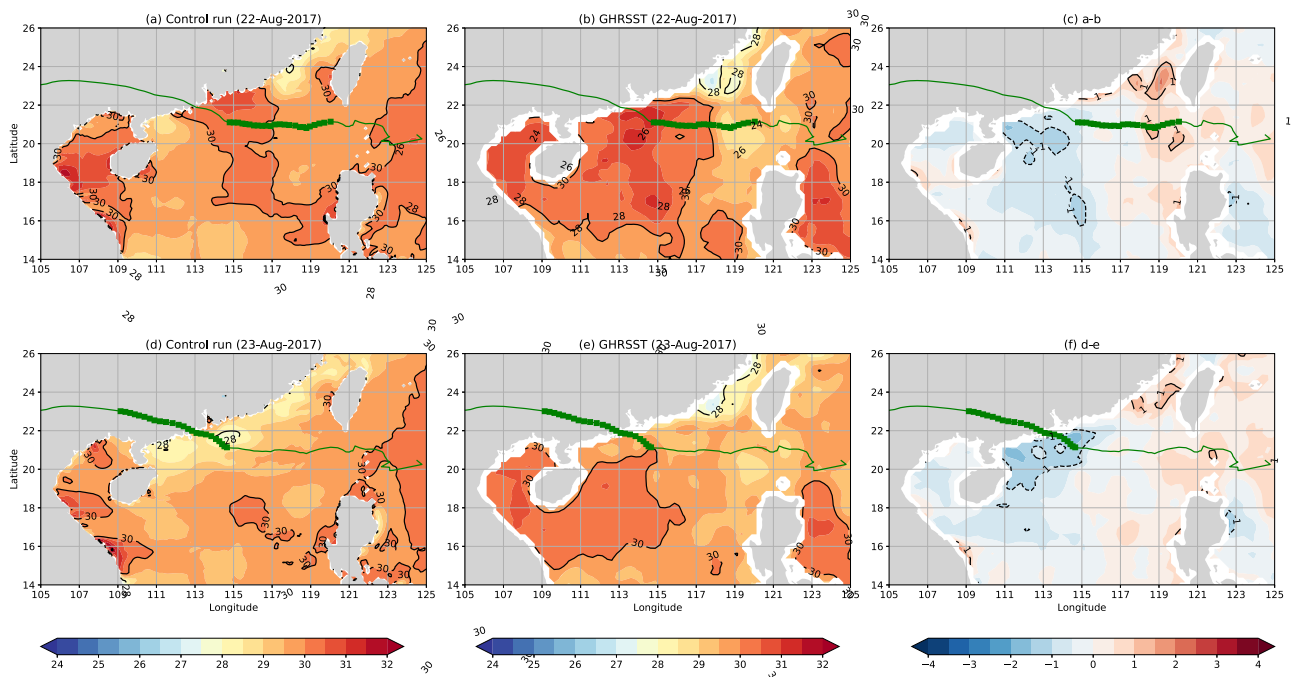


Fig. 10 Comparison of simulated SST and GHRSST. Daily mean SST in °C from **a, d** the control experiment and **b, e** the GHRSST-ABOM dataset. **c, f** SST differences in °C between the model and the GHRSST dataset. **a-c** and **d-f** are dated on 22 and 23 August 2017 respectively. Green lines are the track of Typhoon Hato, highlighted with squares on the corresponding date.

cumulus convection in the outer domain, the Rapid Radiative Transfer Model³⁰ for radiations and the revised MM5 similarity scheme³¹ for the surface layer. The model has two stationary domains covering East Asia and northern South China Sea respectively (red and green boxes in Fig. 9). The horizontal resolution of the outer (inner) domain is 12 km (4 km), with dynamic time step of 30 s (10 s). There are 37 vertical levels from the surface up to 20 hPa.

ROMS is a free-surface, bathymetry-following model, solving the Reynolds-averaged Navier-Stokes equations under the hydrostatic and incompressible

assumptions for the ocean²⁴. The model has a single domain of 6 km horizontal resolution, covering the north South China Sea (blue box in Fig. 9). There are 21 sigma levels with higher resolution above 200 m depth.

The SWAN model solves the wave action balance equation, including physical processes of wind-growth, whitecapping, wave breaking, bottom friction and nonlinear wave-wave interactions²⁵. The model run in non-stationary mode with a time step of 2 min and has a spectral grid of 36 directions (10° resolution) and 25 frequencies. Its domain is the same as ROMS.

The coupled modeling system exchanges information through the MCT²⁶. WRF obtains SST from ROMS, and in return provide states of the atmosphere at the boundary and heat fluxes back to ROMS. WRF also feeds the surface winds to SWAN, and receives states of sea-wave to modify the friction velocity. Ocean currents from ROMS and wave energy dissipation from SWAN are shared between two models.

Experiment designs. COAWST is run for 96 h for three TCs making landfall near Macau: Typhoon Nida (2016), Typhoons Hato (2017) and Mangkhut (2018), and it starts at 00 UTC 31 July 2016, 21 August 2017 and 14 September 2018, respectively, all ~48 h ahead of the observed time of landfall. To ensure consistency between the atmosphere and the ocean, the NCEP Climate Forecast System³² model output initialized at the same time is used to provide the initial and boundary conditions for WRF and ROMS.

Two model runs are made for all TCs: the control run using the configurations mentioned in the previous part, and the NORAD run which both shortwave and longwave radiations are only considered in WRF but not ROMS, i.e., the radiative terms in ROMS are disabled. For Typhoon Hato, an extra simulation NORAD-t18 is preformed, in which the radiative heating terms are only disabled for the first 18 h, i.e., between 00 and 18 UTC on 21 August such that no sunlight enters the ocean for one local day.

Validating SST simulation. Because this study hinges on the correct simulation of the SST, it is important to verify that the model can simulate the actual SST. The simulated daily mean SSTs in the case of Typhoon Hato are therefore compared with the observed SST from the Group for High Resolution Sea Surface Temperature dataset prepared by the Australian Bureau of Meteorology³³ (Fig. 10). The model reproduces similar SST distribution as observed on both days, with a root mean square error of 0.56 °C. These results indicate that the simulations can be used to investigate changes of SST during the passage of Hato.

Data availability

NCEP Climate Forecast System Operational Forecasts 6-Hourly Products are used to force the COAWST model. The data for simulating Typhoon Hato are <https://www.ncei.noaa.gov/data/climate-forecast-system/access/operational-9-month-forecast/6-hourly-by-pressure/2017/201708/20170821/2017082100/>, <https://www.ncei.noaa.gov/data/climate-forecast-system/access/operational-9-month-forecast/6-hourly-ocean/2017/201708/20170821/2017082100/> and <https://www.ncei.noaa.gov/data/climate-forecast-system/access/operational-9-month-forecast/6-hourly-flux/2017/201708/20170821/2017082100/>. For Typhoon Nida, <https://www.ncei.noaa.gov/data/climate-forecast-system/access/operational-9-month-forecast/6-hourly-by-pressure/2016/201607/20160731/2016073100/>, <https://www.ncei.noaa.gov/data/climate-forecast-system/access/operational-9-month-forecast/6-hourly-ocean/2016/201607/20160731/2016073100/> and <https://www.ncei.noaa.gov/data/climate-forecast-system/access/operational-9-month-forecast/6-hourly-flux/2016/201607/20160731/2016073100/>. For Typhoon Mangkhut, <https://www.ncei.noaa.gov/data/climate-forecast-system/access/operational-9-month-forecast/6-hourly-by-pressure/2018/201809/20180914/2018091400/>, <https://www.ncei.noaa.gov/data/climate-forecast-system/access/operational-9-month-forecast/6-hourly-ocean/2018/201809/20180914/2018091400/> and <https://www.ncei.noaa.gov/data/climate-forecast-system/access/operational-9-month-forecast/6-hourly-flux/2018/201809/20180914/2018091400/>. The sea surface temperature dataset used for validation is Australian Bureau of Meteorology (2019) BLUElink Global Australian Multi-Sensor SST Analysis (GAMSSA), daily, 1/4 degree resolution. Ver. 1.0. PO.DAAC, CA, USA. Dataset accessed (10 August 2021) at <https://doi.org/10.5067/GHGAM-4FA1A>. JTWC best track is available at <https://www.metoc.navy.mil/jtwc/jtwc.html?western-pacific>. All COAWST model output are available upon request.

Code availability

COAWST model is downloaded at: https://coawstmodel-trac.sourcerepo.com/coawstmodel_COAWST/. All scripts to reproduce figures from the model outputs are available at <https://doi.org/10.5281/zenodo.5266350>.

Received: 15 February 2021; Accepted: 12 August 2021;

Published online: 02 September 2021

References

- Miyamoto, Y. & Takemi, T. A triggering mechanism for rapid intensification of tropical cyclones. *J. Atmos. Sci.* **72**, 2666–2681 (2015).
- Kowch, R. & Emanuel, K. Are special processes at work in the rapid intensification of tropical cyclones? *Mon. Weather Rev.* **143**, 878–882 (2015).
- Cheng, C. & Wu, C. The role of WISHE in the rapid intensification of tropical cyclones. *J. Atmos. Sci.* **77**, 3139–3160 (2020).
- Balaguru, K. et al. Pronounced impact of salinity on rapidly intensifying tropical cyclones. *Bull. Am. Meteorol. Soc.* **101**, E1497–E1511 (2020).
- DeMaria, M., Sampson, C. R., Knaff, J. A. & Musgrave, K. D. Is tropical cyclone intensity guidance improving? *Bull. Am. Meteorol. Soc.* **95**, 387–398 (2014).
- Emanuel, K. & Zhang, F. On the predictability and error sources of tropical cyclone intensity forecasts. *J. Atmos. Sci.* **73**, 3739–3747 (2016).
- Hong Kong Observatory (2019): Tropical Cyclone in 2017. Hong Kong. <https://www.hko.gov.hk/en/publica/tc/files/TC2017.pdf> (Accessed 10 Aug 2021).
- Pun, I.-F. et al. Rapid intensification of Typhoon Hato (2017) over shallow water. *Sustainability* **11**, 3709 (2019).
- Price, J. F. Upper ocean response to a hurricane. *J. Phys. Oceanogr.* **11**, 153–175 (1981).
- Schade, L. R. & Emanuel, K. A. The ocean's effect on the intensity of tropical cyclones: results from a simple coupled atmosphere–ocean model. *J. Atmos. Sci.* **56**, 642–651 (1999).
- Chan, J. C. L., Duan, Y. & Shay, L. K. Tropical cyclone intensity change from a simple ocean–atmosphere coupled model. *J. Atmos. Sci.* **58**, 154–172 (2001).
- Cione, J. J. & Uhlhorn, E. W. Sea surface temperature variability in hurricanes: implications with respect to intensity change. *Mon. Weather Rev.* **131**, 1783–1796 (2003).
- Vincent, E. M. et al. Assessing the oceanic control on the amplitude of sea surface cooling induced by tropical cyclones. *J. Geophys. Res.: Ocean* **117**, C05023 (2012).
- Zhang, Z., Wang, Y., Zhang, W. & Xu, J. Coastal ocean response and its feedback to Typhoon Hato (2017) over the South China Sea: a numerical study. *J. Geophys. Res.: Atmos.* **124**, 13731–13749 (2019).
- Smith, M. & Toumi, R. A dipole of tropical cyclone outgoing long-wave radiation. *Q. J. R. Meteorol. Soc.* **147**, 166–180. <https://doi.org/10.1002/qj.3912> (2020).
- Warner, J. C., Armstrong, B., He, R. & Zambon, J. B. Development of a coupled ocean–atmosphere–wave–sediment transport (COAWST) modeling system. *Ocean Model.* **35**, 230–244 (2010).
- Dare, R. A. & McBride, J. L. Sea surface temperature response to tropical cyclones. *Mon. Weather Rev.* **139**, 3798–3808 (2011).
- Kara, A. B., Rochford, P. A. & Hurlburt, H. E. An optimal definition for ocean mixed layer depth. *J. Geophys. Res.* **105**, 16803–16821 (2000).
- Frankignoul, C. Sea surface temperature anomalies, planetary waves, and air–sea feedback in the middle latitudes. *Rev. Geophys.* **23**, 357–390 (1985).
- Stramma, L., Cornillon, P., Weller, R. A., Price, J. F. & Briscoe, M. G. Large diurnal sea surface temperature variability: satellite and in situ measurements. *J. Phys. Oceanogr.* **16**, 827–837 (1986).
- Soloviev, A. V. & Lukas, R. Observation of large diurnal warming events in the near-surface layer of the western equatorial Pacific. *Deep Sea Res.* **44**, 1055–1076 (1997).
- Frank, W. M. & Ritchie, E. A. Effects of vertical wind shear on the intensity and structure of numerically simulated hurricanes. *Mon. Weather Rev.* **129**, 2249–2269 (2001).
- Skamarock, W. C. et al. A description of the advanced research WRF version 3. National Center for Atmospheric Research, NCAR Technical Note TN-475+STR, <https://doi.org/10.5065/D68S4MVH> (Boulder, Colorado, United States, 2008).
- Shchepetkin, A. F. & McWilliams, J. C. The regional oceanic modeling system (ROMS): a split-explicit, free-surface, topography-following-coordinate oceanic model. *Ocean Model.* **9**, 347–404 (2005).
- Booij, N., Ris, R. C. & Holthuijsen, L. H. A third-generation wave model for coastal regions: 1. model description and validation. *J. Geophys. Res. Oceans* **104**, 7649–7666 (1999).
- Larson, J., Jacob, R. & Ong, E. The model coupling toolkit: a new fortran90 toolkit for building multiphysics parallel coupled models. *Int. J. High Perform. Comput. Appl.* **19**, 277–292 (2005).
- Hong, S.-Y. & Lim, J.-O. J. The WRF single-moment 6-class microphysics scheme. *J. Korean Meteorol. Soc.* **42**, 129–151 (2006).
- Hong, S.-Y., Noh, Y. & Dudhia, J. A new vertical diffusion package with an explicit treatment of entrainment processes. *Mon. Weather Rev.* **134**, 2318–2341 (2006).
- Tiedtke, M. A comprehensive mass flux scheme for cumulus parameterization in large-scale models. *Mon. Weather Rev.* **117**, 1779–1800 (1989).
- Iacono, M. J. et al. Radiative forcing by long-lived greenhouse gases: calculations with the AER radiative transfer models. *J. Geophys. Res. Atmos.* **113**, D13103 (2008).
- Jiménez, P. A. et al. A revised scheme for the WRF surface layer formulation. *Mon. Weather Rev.* **140**, 898–918 (2012).
- Saha, S. et al. The NCEP climate forecast system version 2. *J. Clim.* **27**, 2185–2208 (2014).
- Zhong, A. & Beggs, H. (2008). Operational implementation of global Australian multi-sensor sea surface temperature analysis. *Anal. Predic. Oper. Bull.*, 77 <http://www.bom.gov.au/australia/charts/bulletins/apob77.pdf> (Accessed 10 Aug 2021).

Acknowledgements

This research was supported by the Hong Kong Research Grants Council General Research Fund E-CityU101/16. R.T. was supported by the UK Met Office Climate

Science for Service Partnership (CSSP) China as part of the Newton Fund. We would also like to thank the two anonymous reviewers for their valuable feedbacks.

Author contributions

C.C.F.L. and J.C.L.C. conceived the idea and co-wrote the manuscript. R.T. contributed in the discussion of the results and editing of the manuscript.

Competing interests

The authors declare no competing interests.

Additional information

Correspondence and requests for materials should be addressed to J.C.L.C.

Peer review information *Communications Earth & Environment* thanks the anonymous reviewers for their contribution to the peer review of this work. Primary Handling Editors: Joy Merwin Monteiro, Joe Aslin and Heike Langenberg.

Reprints and permission information is available at <http://www.nature.com/reprints>

Publisher's note Springer Nature remains neutral with regard to jurisdictional claims in published maps and institutional affiliations.



Open Access This article is licensed under a Creative Commons Attribution 4.0 International License, which permits use, sharing, adaptation, distribution and reproduction in any medium or format, as long as you give appropriate credit to the original author(s) and the source, provide a link to the Creative Commons license, and indicate if changes were made. The images or other third party material in this article are included in the article's Creative Commons license, unless indicated otherwise in a credit line to the material. If material is not included in the article's Creative Commons license and your intended use is not permitted by statutory regulation or exceeds the permitted use, you will need to obtain permission directly from the copyright holder. To view a copy of this license, visit <http://creativecommons.org/licenses/by/4.0/>.

© The Author(s) 2021